Solvation Forces Between Silica Bodies in Supercritical Carbon Dioxide

ARTICLE *in* LANGMUIR · OCTOBER 2008

Impact Factor: 4.46 · DOI: 10.1021/la8010508 · Source: PubMed

3 AUTHORS, INCLUDING:

Yangyang Shen

Rutgers, The State University of New Jersey

12 PUBLICATIONS **47** CITATIONS

SEE PROFILE

Maria Silvina Tomassone

Rutgers, The State University of New Jersey

99 PUBLICATIONS **928** CITATIONS

SEE PROFILE

Solvation Forces Between Silica Bodies in Supercritical Carbon Dioxide

Aleksey Vishnyakov, Yangyang Shen, and M. Silvina Tomassone*

Department of Chemical and Biochemical Engineering, Rutgers, the State University of New Jersey, 98 Brett Road, Piscataway, New Jersey 08854

Received April 3, 2008. Revised Manuscript Received September 11, 2008

We report Monte Carlo simulations of the solvation pressure between two planar surfaces, which represent the interface of spherical silica nanoparticles in supercritical carbon dioxide. Carbon dioxide (CO_2) was modeled as an atomistic dumbbell or a spherical Lennard-Jones particle. The interaction between CO_2 molecules and silica surfaces was characterized by the standard Steele potential with energetic heterogeneities representing the hydrogen bonds. The parameters for the solid−fluid interaction potentials were obtained by fitting our simulations to the experimental isotherms of CO_2 sorption on mesoporous siliceous materials. We studied the dependence of the solvation force on the distance between planar silica surfaces at $T = 318$ K, at equilibrium bulk pressures p_{bulk} ranging from 69 to 200 atm. At 69 atm, we observed a long-range attraction between the two surfaces, and it vanished when the pressure was increased to 102 and then 200 atm. The results obtained with different fluid models were consistent with each other. According to our observations, energetic heterogeneities of the surface have negligible influence on the solvation pressure. Using the Derjaguin approximation, we calculated the solvation forces between spherical silica nanoparticles in supercritical CO_2 from the solvation pressures between the planar surfaces.

1. Introduction

Nanoparticles have been widely utilized to improve material properties, such as mechanical, optical, electrical, and magnetic properties. However, nanoparticles easily aggregate because of their small size and large surface area. The agglomeration of nanoparticles makes them unusable for the synthesis of nanoparticle-based composites, and ultimately destroys those unique properties. Currently, the most popular methods for nanoparticle deagglomeration essentially rely on the shearing of nanoparticle suspensions in organic solvents,[1,2] and this is often facilitated by surfactants/dispersants.[3,4] Another novel route to the deagglomeration of nanoparticles is the rapid expansion of supercritical solutions (RESS). Supercritical fluids have liquid-like density and solubility, yet gas-like diffusivity and viscosity. In the RESS procedure, nanoparticle agglomerates are placed in a supercritical solution; then the solution is rapidly expanded through a nozzle. At high pressure, the fluid adsorbed in the pores inside the agglomerate evaporates rapidly, and a strong shear force is created, which leads to the destruction of agglomerates. This technique is well established for the synthesis of micron- and submicron-size particles.[5,6] For most RESS applications, carbon dioxide is by far the most attractive supercritical fluid, because it is a nontoxic, nonflammable, and inexpensive fluid having convenient critical conditions ($T_c = 304.25$ K, $P_c = 7.38$ MPa).[7] Employment of supercritical CO_2 makes RESS an environmentally friendly alternative to the traditional techniques. For example, RESS was successfully applied to the mixing of 13 nm alumina and 25 nm silica nanoparticles.[8] A continuous-flow RESS apparatus has also been used to grow a magnetic thin film of both nano- and submicronic iron oxide particles under ambient and vacuum conditions.[9] Although the RESS procedure has been employed extensively in the formation and deagglomeration of nanoparticles, further development of this approach requires fundamental understanding of the interaction between nanoparticles in the supercritical fluids. Quantification of these static and dynamics forces would allow deeper insight into the mechanism of the breakup of nanoparticle agglomerates.

The long-range interaction forces between colloidal particles are historically described by the classical theory of Derjaguin, Landau, Verwey, and Overbeek (DLVO) in terms of electrical double layers. When particles are immersed in a fluid and two surfaces approach closer than a few nanometers, they experience fluid-mediated interactions, resulting from the confinement of the fluid between surfaces. These interactions are generally called "solvation forces", which is the key quantity governing the behavior of nanoparticle agglomerates. In the past several decades, accurate and direct measurements of the forces acting between particles as a function of the surface separation in liquids have been performed. Experimentally, the atomic force microscope (AFM) and the surface force apparatus (SFA) are the powerful devices for measurements of interaction forces between two surfaces in fluids;[10] however, the applications to nanoparticles are technically complicated. Molecular simulations, such as Monte Carlo (MC) and molecular dynamics (MD), can be useful in resolving the forces between nanoparticles. Most simulation studies of colloidal nanoparticles were aimed at understanding the hydration forces between nonpolar solutes in water.[11,12] MC

* Author to whom correspondence should be addressed. E-mail: silvina@soemail.rutgers.edu.

(1) Laitinen, N.; Juppo, A. M. *Eur. J. Pharm. Biopharm.* **2003**, *55*(1), 93–98.
(2) Suri, P.; Atre, S. V.; German, R. M.; de Souza, J. P. *Mater. Sci. Eng. A: Struct. Mater. Prop. Microstruct. Process.* **2003**, *356*(1−2), 337–344.
(3) Uhland, S. A.; Cima, M. J.; Sachs, E. M. *J. Am. Ceram. Soc.* **2003**, *86*(9), 1487–1492.
(4) Osman, M. A.; Rupp, J. E. P.; Suter, U. W. *Polymer* **2005**, *46*(19), 8202–8209.
(5) Chang, C. J.; Randolph, A. D. *AIChE J.* **2004**, *35*(11), 1976–1882.
(6) Matsuyama, K.; Mishima, K.; Umemoto, H.; Yamaguchi, S. *Environ. Sci. Technol.* **2001**, *35*(20), 4149–4155.
(7) Altunin, V. V. *IUPAC. International Thermodynamic Tables of the Fluid State*; Pergamon Press: London, 1976; Vol. *3*.
(8) Yang, J.; Wang, Y.; Dave, R. N.; Pfeffer, R. *Adv. Powder Technol.* **2003**, *14*(4), 471–493.
(9) De Dea, S.; Graziani, D.; Miller, D. R.; Continetti, R. E. *J. Supercrit. Fluids* **2007**, *42*(3), 410–418.
(10) Israelachvili, J. N. *Intermolecular and Surface Forces*; Academic Press: London/San Diego, 1991.
(11) Wallqvist, A.; Berne, B. J. *J. Phys. Chem.* **1995**, *99*(9), 2893–2899.
(12) Bolhuis, P. G.; Chandler, D. *J. Chem. Phys.* **2000**, *113*(18), 8154–8160.

10.1021/la8010508 CCC: $40.75
Published on Web 10/28/2008

and MD simulation methods have also been used previously to explore the solvation forces in slit-like pore filled with hard spheres, Lennard-Jones (LJ) fluids, water, alkanes,[13] and polymers at "gas-like" and "liquid-like" polymer densities.[14] A few recent papers report MD modeling of two nanoparticles in LJ and soft-sphere fluids. Shinto et al.[15] varied the solid−fluid interactions to study the van der Waals and solvation forces between liophobic and liophilic nanoparticles. Qin and Fichthorn[16,17] also performed similar studies in which they represented the nanoparticles as rigidly fixed clusters of LJ atoms and determined the effect of particle size, shape, and roughness on the solvation forces. The force profiles between two nanoparticles obtained in all these studies are similar in form to those predicted for fluids confined between flat and infinite surfaces (attractive for liophobic and oscillatory for liophilic nanoparticles).[18−20] Bedrov et al.[21] simulated solvation forces between fullerenes and carbon nanotubes in water and found deviations from standard hydrophobic behavior. Other simulation studies focused on the forces between nanostructured surfaces commented by liquid junctions.[22,23]

In all these previous publications, the focus was on solvation forces between nanoparticles in *vapors and liquids,* but not in *supercritical fluids*. In vapors, the adsorption field of the two bodies typically leads to the formation of a liquid-like junction between them. The solvation forces can be interpreted in terms of the surface tension of the formed meniscus, and essentially vanishes when the junction breaks up. The other group of simulation studies deals with solvation forces between planar surfaces and particles in liquids and polymers. Neither of these groups accounts for the specifics of a dense supercritical fluid, where meniscus formation is not really possible (unlike vapors), but strong density variations frequently occur (unlike liquids).

The purpose of this paper is to gain a fundamental understanding of the interparticle forces in supercritical fluids, and to practically evaluate the solvation forces between silica nanoparticles in supercritical CO_2, in order to estimate the breakup barriers in the RESS deagglomeration and mixing procedures. Despite their small size, nanoparticles are often still too large for direct atomistic simulations of the interparticle forces. Thus we attempt to derive the solvation forces from the profiles of the normal component of the pressure tensor in slit pores formed by planar surfaces whose properties are similar to those of silica nanoparticles (except shape). We explore the solvation forces between two silica nanoparticles in CO_2 at supercritical temperature $T = 318$ K and pressures $p = 69-200$ atm. To calculate the solvation forces between the larger particles (20−60 nm in diameter), we first study the disjoining pressure between two planar silica surfaces, and then the solvation force between spherical surfaces of similar properties is derived via the Derjaguin approximation. The Derjaguin approximation assumes that the distance between particles is substantially larger than the molecular diameter, but is small compared to the particle size. For spherical surfaces, this approximation states that the interaction force is proportional to their effective radius, where the inverse effective radius is defined as the arithmetic mean of the inverse curvature radii of the surfaces involved. The Derjaguin approximation is applicable as long as the range of the interaction and the separation distance is small compared to the radii of curvature.

The organization of this paper is as follows: the models used in this work, simulation setup and calculation methods are described in Section 2. In Section 3, we examine the dependence of solvation pressures on several factors, such as bulk pressure, fluid model, and surface inhomogeneity under the supercritical conditions. Then the solvation forces between large and spherical nanoparticles are derived via the Derjaguin approximation. Finally a brief conclusion is presented in Section 4.

2. Models and Methods

2.1. CO_2 Dumbbell and LJ Models. We followed the well-established approach for choosing intermolecular potentials by Ravikovitch et al.[24] Here the fluid force field is chosen to reproduce the bulk phase diagram at similar conditions, while the solid-fluid interactions are fitted to the experimental sorption isotherms on nonporous or mesoporous surfaces. In this work, we utilized the CO_2 model of Möller and Fischer[25] (from now on referred to as the *dumbbell* model), which combines two LJ pseudoatoms connected by a rigid bond with a point quadrupole located in the center. This model accurately describes the liquid−vapor equilibrium properties and the saturation pressures of bulk CO_2 at subcritical temperatures.[26] We performed a series of gauge cell MC[27,28] simulations and constant-pressure (NPT) MD simulations of bulk CO_2 at $T = 323.15$K and $p < 105$ atm and verified that the model reproduces quite reasonably the bulk PVT data.[29] We also employed a simpler LJ model for bulk CO_2 with the LJ parameters σ and ε found from fitting the Johnson's equation of state[30] for LJ fluid to the experimental bulk isotherm at 323.15 K.[29] The simple LJ model gives an excellent agreement with the experimental isotherm up to very high pressures (Figure 1).[31]

2.2. CO_2 Interactions with Silica. The interactions between CO_2 molecules and silica were characterized in terms of the sorption isotherms on the nonporous or mesoporous silica surfaces. Published experimental data about the adsorption of CO_2 on amorphous silica both at cryogenic and room temperatures show significant dependence of CO_2 sorption on surface hydroxylation due to the hydrogen bond formation between the surface hydroxyls and CO_2 oxygen atoms.[32,33] In this work, we considered the strongly hydroxylated silica surfaces. We chose the isotherms on FSM-10 mesoporous silica at the CO_2 critical temperature of 303 K[33] and the low-temperature isotherms on MCM-41 mesoporous molecular sieves as references. The critical

(13) Dijkstra, M. *Thin Solid Films* **1998**, *330*(1), 14–20.
(14) Yethiraj, A.; Hall, C. K. *Macromolecules* **1990**, *23*(6), 1865–1872.
(15) Shinto, H.; Miyahara, M.; Higashitani, K. *J. Colloid Interface Sci.* **1999**, *209*, 79–85.
(16) Qin, Y.; Fichthorn, K. A. *J. Chem. Phys.* **2003**, *119*(18), 9745–9754.
(17) Qin, Y.; Fichthorn, K. A. *Phys. Rev. E* **2006**, *73*(2), 020401.
(18) Snook, I. K.; van Megen, W. *J. Chem. Phys.* **1980**, *725*, 2907–2913.
(19) Wang, Y.; Hill, K.; Harris, J. G. *J. Chem. Phys.* **1994**, *100*(4), 3276–3285.
(20) Gao, J.; Luedtke, W. D.; Landman, U. *Phys. Rev. Lett.* **1997**, *79*, 705–708.
(21) Li, L.; Bedrov, D.; Smith, G. D. *J. Phys. Chem. B* **2000**, *110*(21), 10509–10513.
(22) Jang, J. Y.; Ratner, M. A.; Schatz, G. C. *J. Phys. Chem. B* **2006**, *110*(2), 659–662.
(23) Schoen, M. *Colloids Surf., A: Physicochem. Eng. Aspects* **2002**, *206*(1−3), 253–266.
(24) Ravikovitch, P. I.; Vishnyakov, A.; Russo, R.; Neimark, A. V. *Langmuir* **2000**, *16*(5), 2311–2320.
(25) Möller, D.; Fischer, J. *Fluid Phase Equilib.* **1994**, *100*, 35–61.
(26) Vrabec, J.; Stoll, J.; Hasse, H. *J. Phys. Chem. B* **2001**, *105*(48), 12126–12133.
(27) Neimark, A. V.; Vishnyakov, A. *J. Chem. Phys.* **2005**, *122*(23), 234108.
(28) Vishnyakov, A.; Neimark, A. V. *J. Phys. Chem. B* **2001**, *105*(29), 7009–7020.
(29) Span, R.; Wagner, W. *J. Phys. Chem. Ref. Data* **1996**, *25*(6), 1509–1596.
(30) Johnson, J. K.; Zollweg, J. A.; Gubbins, K. E. *Mol. Phys.* **1993**, *78*(3), 591–618.
(31) Vishnyakov, A.; Shen, Y.; Tomassone, M. S. *J. Chem. Phys.*, submitted for publication, 2008.
(32) Bakaev, V. A.; Steele, W. A.; Bakaeva, T. I.; Pantano, C. G. *J. Chem. Phys.* **1999**, *111*(21), 9813–9821.
(33) Katoh, M.; Sakamoto, K.; Kamiyamane, M.; Tomida, T. *Phys. Chem. Chem. Phys.* **2000**, *2*(19), 4471–4474.

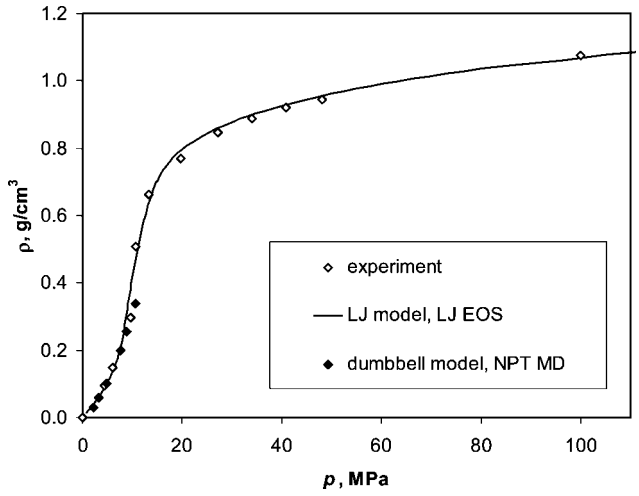

Figure 1. CO_2 bulk isotherm (density vs pressure) at $T = 323.15$K. Experimental data is from ref 29. The data for the LJ model was obtained using the LJ equation of state.[30] The isotherm for the dumbbell model was obtained using constant-pressure MD simulations.

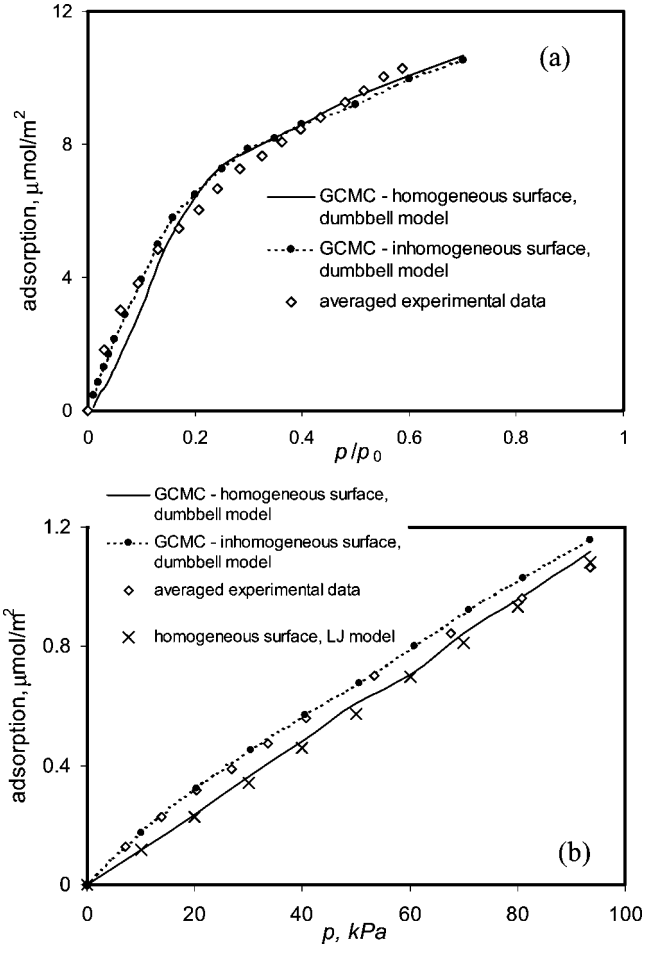

Figure 2. Calculated (GCMC) and reference isotherms of CO_2 sorption on hydroxylated amorphous silica surface at 195 K (a) and 303 K (b). The reference isotherm at 195 K is the average of the experimental isotherms of Bhatia et al.[43] and Morishige et al.;[44] the reference isotherm at 303 K was taken from ref 33.

temperature isotherms exhibit submonolayer surface coverage by CO_2 below 1 atm and show visible curvature (Figure 2). The behavior originates from the surface heterogeneity, which may be related to the different arrangements of the hydroxyl groups. The low-temperature isotherms on strongly hydroxylated samples show a distinct monolayer region; however, the distinct monolayer transition, visible on graphitized carbons,[32,34,35] is not clearly seen on silica. This can be explained by the surface inhomogeneity.

2.3. Solid−Fluid Potentials. The solid−fluid interactions are fitted to the experimental sorption isotherms on nonporous or mesoporous surfaces. The standard Steele potential is our starting point. Each LJ center of the CO_2 molecule interacts with each silica surface via the 10-4-3 potential of Steele:[36]

$$U_{sf}(z) = 2\pi\rho_s\varepsilon_{sf}\sigma_{sf}^2\Delta\left[\frac{2}{5}\left(\frac{\sigma_{sf}}{z}\right)^{10} - \left(\frac{\sigma_{sf}}{z}\right)^4 - \frac{\sigma_{sf}^4}{3z(z+0.61\Delta)^3}\right] \quad (1)$$

where ρ_s is the *volume* density of the LJ pseudoatoms in the lattice, Δ is the distance between the layers in the lattice, ε_{sf} and σ_{sf} are the LJ parameters for the solid-fluid interactions, and z is the distance between the fluid molecule and the plane that contains the surface centers of the atoms of the solid. First, we adjusted the parameters of the Steele potential σ_{sf} and ε_{sf} for both the dumbbell and LJ CO_2 models from the best fit of the isotherms of CO_2 sorption on the model surface to the experimental data at critical and cryogenic temperatures (Figure 2). However, the structureless model of the solid was unable to adequately describe the experimental adsorption isotherm of CO_2 on MCM-41 at low pressures (Figure 2). The critical pressure isotherm below the atmospheric pressure was nearly linear, while the cryogenic isotherm exhibited a distinct monolayer transition. This transition is typical for crystal surfaces such as graphite[32,34,35] rather than amorphous silica. To account for the surface heterogeneity of amorphous silica, we mimicked a "rough" surface by modifying the fluid−solid energy landscape, placing additional attractive and repulsive sites on the surface, which are randomly distributed.[37] Each site corresponds to a spherical potential well. A sample distribution of the sites over the pore walls is shown in Figure 3. If the center of mass of a CO_2 molecule was found within an inhomogeneity site, a perturbation energy then was added or subtracted from the total solid−fluid energy of the molecule. We used four types of inhomogeneities in each simulation: two attractive and two repulsive (Table 1). This inhomogeneous surface model allowed for a reasonable and accurate reproduction of the reference isotherms (Figure 2).

2.4. Simulation Details. Adsorption/desorption isotherms were simulated using the standard grand canonical Monte Carlo (GCMC) method.[38] The total number of attempted steps was 30 000 per molecule. In all GCMC simulations we used the original algorithm of Norman and Filinov;[39] one insertion and one removal were attempted per one displacement/rotation. The chemical potential in the implicit bulk reservoir corresponded to bulk pressure.

The dependence of the fluid pressure on the chemical potential for the dumbbell model of CO_2 was calculated using the gauge cell method.[28] The molecules were placed in a cubic simulation box of constant volume with 5nm side; gauge cell size was adjusted automatically to contain 50 molecules in average. The chemical potential of CO_2 was calculated from the mean density

(34) Beebe, R. A.; Kiselev, A. V.; Kovaleva, N. V.; Tyson, R. F. S.; Holmes, J. D. *Russ. J. Phys. Chem. (Transl. Zh. Fiz. Khim.)* **1964**, *38*, 372.
(35) Bottani, E. J.; Bakaev, V. A.; Steele, W. A. *Chem. Eng. Sci.* **1994**, *49*(17), 2931–2939.
(36) Steele, W. A. *The Interactions of Gases with Solid Surfaces*; Pergamon Press: Oxford, 1974.
(37) Ravikovitch, P. I.; Vishnyakov, A.; Neimark, A. V.; Ribeiro Carrott, M. M. L.; Russo, P. A.; Carrott, P. J. *Langmuir* **2006**, *22*, 513–516.
(38) Allen, M. P.; Tildesley, D. J. *Computer Simulation of Liquids*; Oxford University Press: Oxford, 1987.
(39) Norman, G. E.; Filinov, V. S. *High Temp. (USSR)* **1969**, *7*, 216–222.

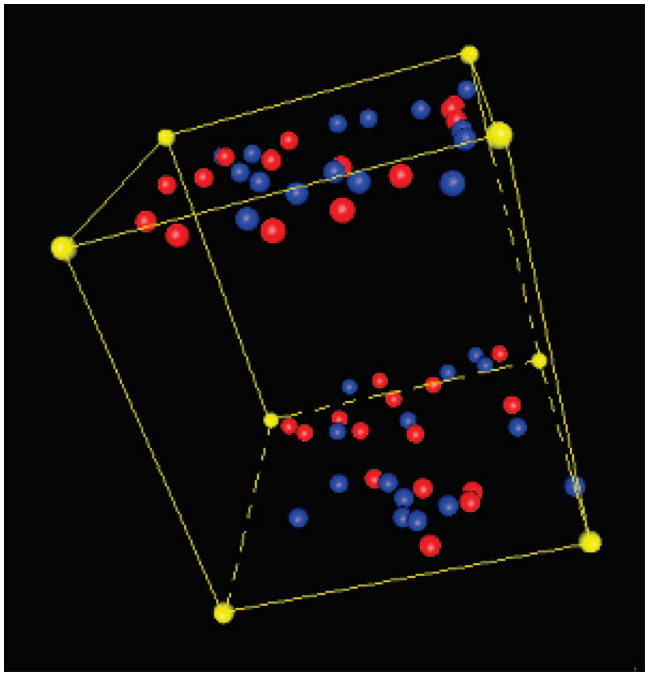

Figure 3. Point surface inhomogeneity: distance between the solute molecule and inhomogeneity versus extra energy added to the "base" 10-4-3. Attractive interaction: blue. Repulsive interaction: red.

Table 1. Parameters of Intermolecular Interactions

model	dumbbell	LJ
	fluid−fluid	
ε_{ff}, kJ/mol	1.04	2.38
σ_{ff}, nm	0.3035	0.368
Q, C·m^2	3.0255	
l, nm	0.212	
	solid−fluid: homogeneous contribution	
$\rho_s\varepsilon_{sf}\Delta\sigma_{sf}^2$, kJ/mol	1.88	2.91
σ_{sf}, nm	3.21	3.43

solid-fluid: inhomogeneities			
ε_{ih}, kJ/mol	ρ_{ih}, μmol/m^2	ε_{ih}, kJ/mol	ρ_{ih}, μmol/m^2
0.9	−4	−19.0	1.22
0.9	−6.2	−9.5	0.61
0.9	−3.1	19.0	1.22
0.9	12.4	9.5	0.61
0.9	6.2		
0.9	3.1		

in the gauge, and the pressure was calculated from the standard virial formula.[38]

2.5. Solvation Pressure and Force. The normal component of the pressure tensor in the pore p_n was calculated as the average force acting from fluid molecules to the surface per unit area.[18] The solvation pressure is the difference between the normal pressure in the pore and the bulk pressure:

$$p_s = p_n - p_{bulk} \quad (2)$$

Since p_{bulk} in eq 2 is constant, it is equivalent to study the solvation pressure or the pressure normal component.

To evaluate the forces between silica nanoparticles from the solvation pressure between two planar surfaces, we employed the Derjaguin approximation,[40] which, as mentioned earlier, is based on the assumptions that the distance between particles is substantially larger than the molecular diameter but is small compared to the particle size. For our target systems (20−50 nm silica particles), these assumptions are very reasonable. Reducing Derjaguin's derivations for identical spherical surfaces, one obtains

$$F(H_0) = \pi R \int_{\infty}^{H_0} p_s(h)\mathrm{d}h \quad (3)$$

where R is the particle radius, and H_0 is the distance between surfaces.

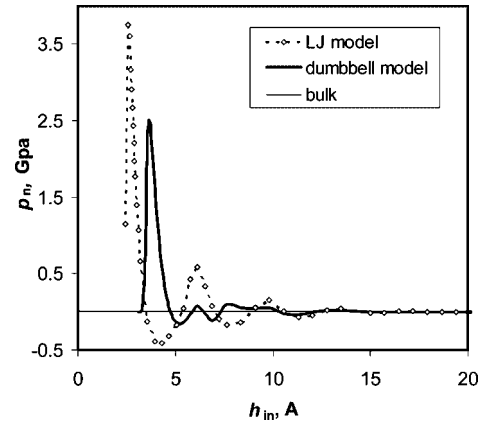

Figure 4. Normal pressure in slit pores as a function of the internal width h_{in} on different adsorbate models (LJ model verus dumbbell model). The pore is formed by homogeneous walls, representing the amorphous silica surfaces. T = 318 K, p_{bulk} = 69 atm.

3. Results and Discussion

In the present work, we have preformed computer simulations via the GCMC method to obtain the normal component of the pressure tensor in the slit pores. Two models of fluid were used: the simple LJ model and the dumbbell model. Three equilibrium bulk pressures were considered: 69 atm, 102 atm, and 200 atm. Two models of pore surface were used: a smooth surface, which interacted with each of the LJ centers of a fluid molecule via the 10-4-3 Steele potential, and an inhomogeneous surface, which contained potential "bumps" and "wells". Then using eq 3, we calculated the solvation forces between silica nanoparticles for each fluid model, equilibrium bulk pressure, and the surface roughness.

3.1. Effect of the Fluid Model. Figure 4 shows the dependence of the normal component of the solvation pressure between two homogeneous silica surfaces (in this case, only the Steele 10-4-3 potential is included in the solid−fluid interactions) at p_{bulk} = 69 atm for both LJ and dumbbell CO_2 models. At small separations between the surfaces, the normal component of the solvation pressure exhibits very strong oscillations, which are related to the fluid layering between the walls. Such behaviors are well documented both in simulations and experiments.[23,41] The peaks, meaning the strongly repulsive solvation forces, correspond to the pore widths when a new layer is formed and the interlayer separation is small, and the minima of the solvation force correspond to the pore widths when the distance between the adjacent layers is large. The locations of the extremes of the normal pressure (or solvation force) strongly depend on the fluid model. For the LJ model, the regular oscillations are clearly shown, and they are visible up to h_{in} = 35 Å. There are as many as 12 layers are formed in the pore. For the dumbbell model, the oscillations flatten quickly (h_{in} > 12 Å) because of the possibility

(40) Chuaev, N. V.; Derjaguin, B. V.; Muller, V. M. *Surface Forces*; Springer: Berlin, 1987.

(41) Gee, M. L.; McGuiggan, P. M.; Israelachvili, J. N.; Homola, A. H. *J. Chem. Phys.* **1990**, *93*(3), 1895–1906.

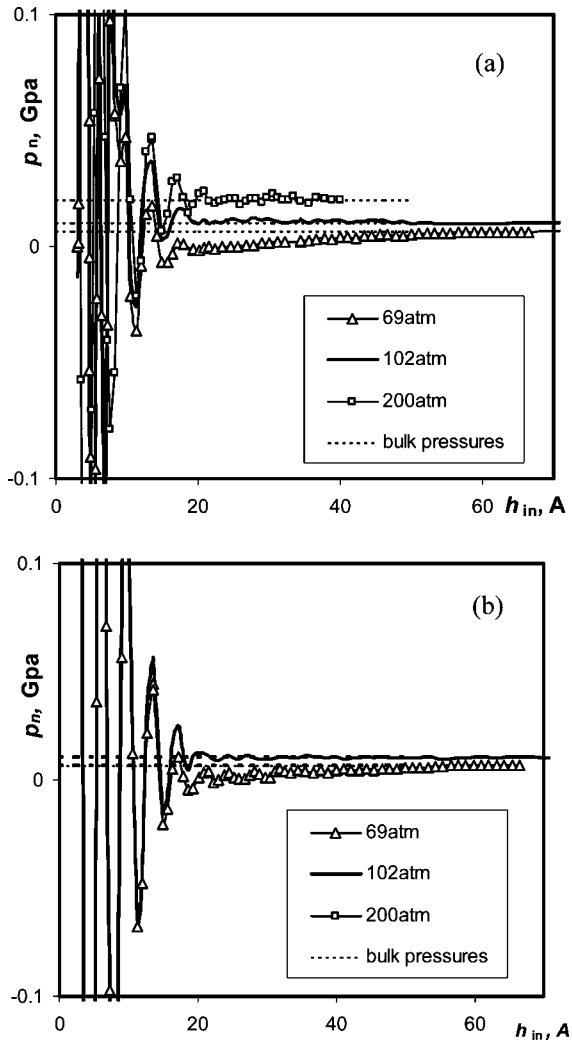

Figure 5. Normal pressure of CO_2 as a function of the pore width for different values of the equilibrium bulk pressure p_{bulk} at $T = 318$ K, for different fluid models: LJ (a) and dumbbell (b). The slit pore is formed by homogeneous walls.

of different orientations of CO_2 molecules in the layers that weaken the layering.

Because the solvation forces at short distances are very sensitive to the surface geometrical roughness,[42] they are not the focus of our studies. In addition, Derjaguin's equation is not applicable in this range of small pore widths. As the oscillations flatten, the normal pressure p_n at $p_{bulk} = 69$ atm for both models emerges negative and increases monotonically to the bulk pressure value, and it approaches to the bulk pressure due to the statistical fluctuations at $h_{in} \approx 40$ Å. The results for the two models are in excellent agreement to each other. This means that the solid−fluid interactions cause significant effective attraction between the surfaces, thus preventing the agglomerates from decomposition.

3.2. Effect of the Equilibrium Bulk Pressure. The differences between the normal component of the solvation pressure dependence on the pore widths at different bulk pressures are depicted in Figure 5, where $p_n(h)$ is shown for three different values of p_{bulk}. In all cases, the normal pressure tends to reach

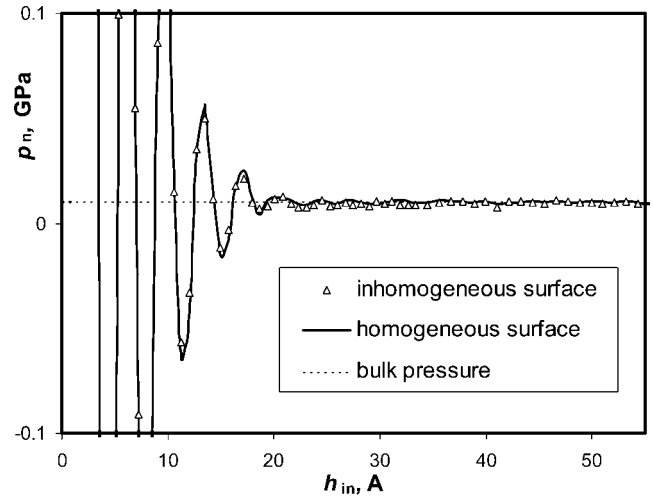

Figure 6. Normal pressure of CO_2 (represented by the dumbbell model) in pores with energetically homogeneous and inhomogeneous walls at $p_{bulk} = 69$ atm.

the bulk pressure value for wider separations considered. For $p_{bulk} = 69$ atm, the normal pressure is lower than the bulk value when the separation is between approximately 15 and 50 Å, suggesting that the surfaces are effectively attractive. This long-range attraction, however, is not observed at higher bulk pressures. For example, at $p_{bulk} = 102$ atm, p_n oscillates around p_{bulk} at $h > 20$ Å, which indicates that the solvation pressure is close to zero. When the bulk pressure is further increased to 200 atm, the normal pressure merges very quickly with the bulk pressure. This behavior indicates the higher the bulk pressure, the weaker the attraction forces, and in turn the deagglomeration process is more feasible. There is no obvious difference between the two higher-pressure cases. The results from all three cases do not depend on the fluid models employed.

3.3. Effect of Surface Roughness. Figure 6 shows the dependence of the normal pressure on the model of solid, i.e., the surface energetic inhomogeneities of the solid walls. It is clear that, unlike the geometric roughness studied in ref 42, the influence of purely energetic inhomogeneities is very minor and only visible at small separations that are out of the focus of this paper. The surface energetic inhomogeneities do not substantially affect the value of the solvation force between the particles.

3.4. Derivation of Solvation Forces. From the profiles of solvation pressure p_s in slit pores, we have estimated the solvation forces between the spherical silica nanoparticles using the Derjaguin approximation. This solvation force does not include the direct attraction between the particles; it only results from the interaction between the particles and the fluid molecules. The nanoparticles used in ref 8 are 50 nm in diameter. According to the Derjaguin equation, the force is proportional to the particle diameter, so the forces between larger particles (or smaller in the range where Derjaguin's approximation is still feasible) can be obtained by scaling. Figure 7 shows the solvation forces calculated at supercritical conditions ($T = 318$ K and two bulk pressures of 69 atm and 102 atm) with two fluid models. At $p_{bulk} = 69$ atm, there exists long-range attraction between nanoparticles, which reaches 2 nN (nanonewtons) at $h = 3.56$ Å. The results with different fluid models do not show a significant difference at this relatively low pressure. While the attraction between nanoparticles at the bulk pressure of $p_{bulk} = 102$ atm is much weaker (it only reaches 1 nN at $h = 6.87$Å) and there is no visible attraction between the particles at the bulk pressure of $p_{bulk} = 200$ atm.

3.5. Effect of CO_2 Fluid Structure Inside Pores of Different Sizes. Figure 8a,b shows the density profiles for pores of 24−56

(42) Frink, L. J. D.; van Swol, F. *J. Chem. Phys.* **1998**, *108*(13), 5588–5598.
(43) Sonwane, C. G.; Bhatia, S. K.; Calos, N. *Ind. Eng. Chem. Res.* **1998**, *37*(6), 2271–2283.
(44) Morishige, K.; Fujii, H.; Uga, M.; Kinukawa, D. *Langmuir* **1997**, *13*(13), 3494–3498.

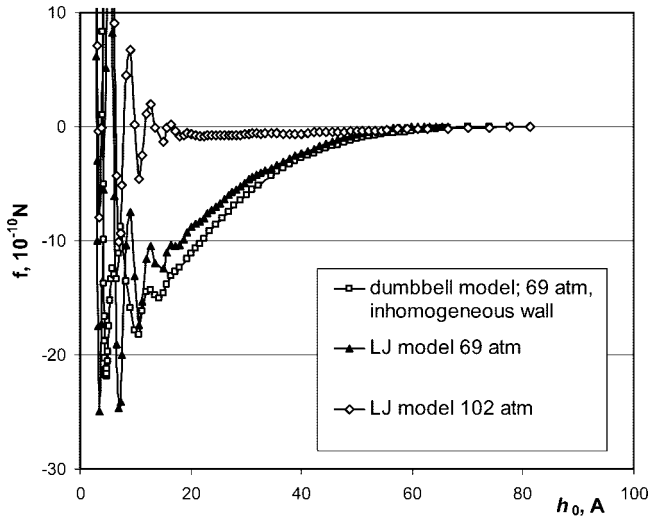

Figure 7. Solvation forces between silica nanoparticles at different bulk pressures at 318 K calculated using the Derjaguin model.

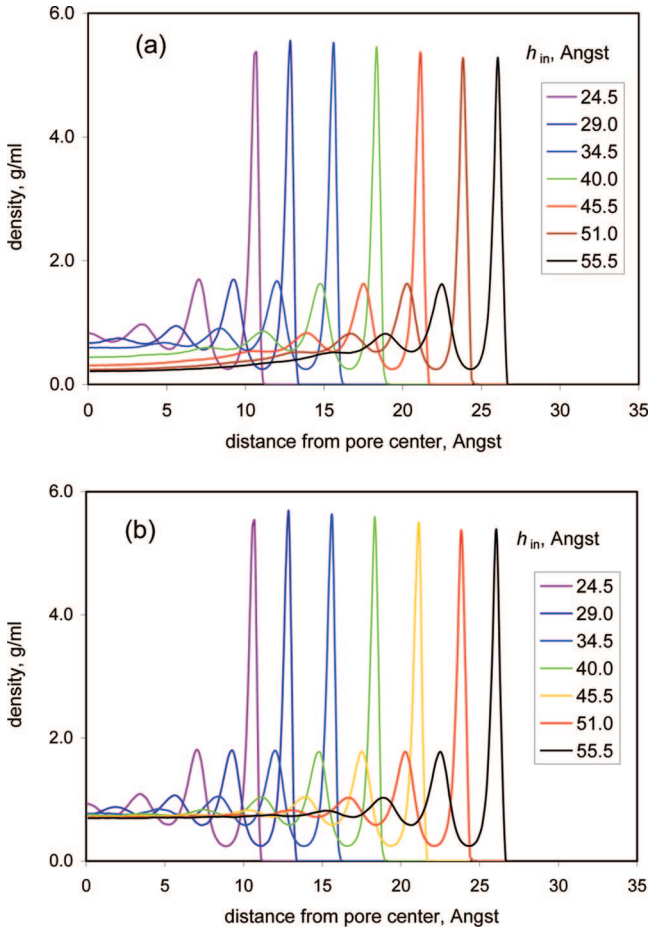

Figure 8. Density profiles for CO_2 in slit pores of different widths obtained with the LJ fluid model. (a) $p_{bulk} = 69$ atm; (b) $p_{bulk} = 102$ atm.

Å widths, where the differences in the solvation force between $p_{bulk} = 69$ atm and higher pressures are most significant. At $p_{bulk} = 69$ atm (Figure 8a), the fluid−solid interactions cause a pronounced densification of the fluid in 20−30 Å pores, where the density in the center is liquid-like (i.e., approximately 0.7 g/cm^3), about four times greater than the bulk's density. It appears that the change in density at supercritical temperatures should lead to higher normal pressure and therefore to an increase in the solvation force. However, since the temperature chosen for this study is not far above the critical point ($p_{bulk}/p_c = 1.05$), the bulk isotherm still resembles those of subcritical fluids. The isotherm has a vapor phase of relatively constant compressibility, followed by a rapid increase in density (Figure 1). Because of a very high compressibility at these pressures, the densification causes only a modest effect on p_n. At the same time, the fluid of liquid-like densities that fills the central part of the pore interacts attractively with the walls, thus reducing p_n. Apparently, this effect outweighs the positive effect mentioned above, which results in a negative solvation force.

At higher bulk pressures the situation is different. For example, Figure 8b shows the density profiles at different distances between the walls at $p_{bulk} = 102$ atm. Even in the central part of the pore where the density fluctuations imposed by the confinement level off, the fluid density is liquid-like and close to that of the bulk fluid for the entire range of pore sizes. This results in a relatively weak dependence of the solvation forces on the pore size, and a lower magnitude of the force, which remains slightly attractive in the entire pore range before it diminishes to zero (i.e., this can be also seen in Figures 5 and 6).

4. Conclusions

We employed GCMC simulations to study the solvation forces between two silica nanoparticles in supercritical CO_2 at $T = 318$ K and a pressure range of 69 to 200 atm (1000 − 3000 psi). Our results show that the solvation force is very sensitive to the bulk fluid pressure. At 69 atm, and we observed a distinct attraction between the particles at the intermediate distances between 3 and 60 Å, which certainly affects the work of the agglomerate formation (or breakdown) in the supercritical CO_2. For two 50 nm nanoparticles at 69 atm, the attractive force reaches 2 nN, and the work of their removal reaches a value of 2.93×10^{-4} fJ at an interparticle distance of 3.56 Å. The attraction becomes much weaker at $p_{bulk} = 102$ atm ($f = 1$ nN and $w = 2.41 \times 10^{-4}$ fJ at a separation of 6.87 Å) and vanishes at $p_{bulk} = 200$ atm.

Our results show that, at $p_{bulk} = 69$ atm, the fluid−solid interactions generate a pronounced densification of the fluid in 20−30 Å pores, and the bulk isotherm still resembles the isotherm of subcritical fluids, first exhibiting a vapor phase of relative constant compressibility, and then, as the density increases, showing a modest increase in the pressure and a negative solvation force. At higher values of the pressure we found a weaker dependence of the solvation forces on the pore size, and a lower magnitude of the force, which is attractive over the entire size range of the pores before it diminishes to zero.

Under such conditions of high pressure, the deagglomeration mechanism might be closer to those in traditional techniques that involve liquid organic solvents. In the case of CO_2 supercritical fluid, an initial stage of liquid-like solvation is followed by a rapid depressurization that makes the deagglomeration even more efficient.

Acknowledgment. We thank Dr. Alexander V. Neimark for stimulating discussions. The work was supported by an NSF NIRT grant, (Nanoscale Interdisciplinary Research Team) # 0506722.

LA8010508